Lumped parameters models of rectangular pneumatic pads: static analysis

Lumped parameters models of rectangular pneumatic pads: static analysis

Federico Colombo, Terenziano Raparelli, Andrea Trivella, Vladimir Viktorov
Politecnico di Torino, Department of Mechanical and Aerospace Engineering
Corso Duca degli Abruzzi 24, Torino, Italy

Abstract

A lumped parameters model of a rectangular pneumatic pad is developed and static analysis is performed. The model can be implemented more quickly than a distributed parameters model and is equally accurate. The influence of geometric parameters is discussed to help the reader in the design of pneumatic pads. Analysis is carried out in dimensionless form to obtain results of general validity.

Keywords: gas bearing, lumped model, pneumatic pad

Nomenclature

α	Dimensionless distance from pad edge
β	Pad aspect ratio
γ	Dimensionless distance between supply holes
μ	Gas viscosity
$\overline{d_s}$	Supply hole diameter
b	Critical pressure ratio
c_d	Supply hole discharge coefficient
d_s	Dimensionless supply hole diameter
h	Air gap
h_{ref}	Reference air gap (=10 μm)
k	Pad stiffness
$\bar{k}$	Dimensionless pad stiffness
k_T	Temperature coefficient, $k_T = \sqrt{\frac{T_0}{T}}$
l	Distance from pad edge
p	Pressure
p_a	Ambient pressure
p_c	Supply hole downstream pressure
p_0	Mean pressure in supply rectangle
p_s	Supply pressure
ρ_0	Air density in normal conditions (p_0=100 kPa and T_0=293.5 K)
w	Distance between supply holes
C	Conductance of the supply hole
F	Pad load capacity
$\bar{F}$	Dimensionless load capacity
Φ	Pressure ratio coefficient
G	Gas mass flow rate
$\bar{G}$	Dimensionless gas mass flow rate
H	Dimensionless air gap
L_x, L_y	Length of pad sides
N_x, N_y	Number of supply holes along x,y directions

P	Dimensionless pressure
R	Gas constant, in calculations =287 J/(kg K)
Re	Reynolds number
T	Absolute temperature, in calculations =293 K
Ψ	Coefficient of isentropic expansion, in calculations $\Psi = \frac{0.685}{\sqrt{R \cdot T}}$
X, Y	Dimensionless axes

1. Introduction

Gas bearings are widely used in precision engineering because of their low friction, oil-free operation and freedom from wear. Accordingly, more and more linear guideways for measuring machines and precision positioning systems are provided with these components. Their design is important in ensuring that the machine meets requirements for load capacity, stiffness, air flow consumption and time response.

Analytical models of flow can be used only for a few simple bearing geometries [1-7]. With the advent of computerized methods, Distributed Parameters (DP) models made it possible to simulate the pressure distribution under the bearings more realistically, in particular for complex geometries. Finite difference methods [8-12] and finite element methods [13-17] have been shown to be capable of calculating bearings of any geometry. A multiphysics finite element model can also be used to consider the interaction between the air flow dynamics and the bearing's structural flexibility, as for example in [18]. Recently, Computational Fluid Dynamics (CFD) was used jointly with experimental activities to improve the description of the flow field near the supply holes [19-23]. In [24,25], by contrast, semi-analytical methods were employed to determine orifice discharge coefficients, which were then used in analytical formulations.

However, DP models can require considerably longer solution times and it is more difficult to identify the dominant factors that influence pad characteristics. With Lumped Parameters (LP) models, only a few values of pressure in the gap are sufficient to calculate the bearing's characteristics. Though LP models yield less accurate results than DP models, they are faster and simpler to implement in the design process and in optimization. Nevertheless, few papers have addressed simplified LP models.

A circular porous thrust bearing is studied using an LP model in [26]. In paper [27], a circular thrust bearing with multiple pocketed orifices was modelled with a simplified calculation method that was found to be faster than DP methods. An integral gas bearing is analyzed in paper [28] with an LP model, providing information about the most appropriate configuration. Paper [29] analyzes rectangular pads with a supply recess. Analysis makes use of simplifying assumptions and an empirical formula which relates the recess pressure to the supply pressure. In paper [30], a lumped model is used to study the behavior of a pneumatic journal bearing.

As far as the authors know, rectangular pads have been investigated in only a few experimental studies [31,32] and in analytical analyses dealing with simplified geometries [33]. The present paper introduces a lumped parameters model that is a practical and sufficiently accurate tool for designing and optimizing rectangular pads with multiple holes. This model is the evolution of a previous model described in papers [34,35]. A rectangular pad shape is considered with different aspect ratios, supply pressures and number and diameter of supply holes. Static results are discussed in dimensionless form. The results of the LP model are compared with those of the DP model and their accuracy is estimated.

2. Pad geometry

Rectangular pads with sides L_x and L_y are considered. Pad geometry is shown in Figure 1. Multiple supply holes are positioned on the sides of a supply rectangle at distance *l* from the edges of the pad. This distance is the same along x and y directions. The holes are equi-spaced at a distance *w*, which is also assumed to be equal along the two directions. The hole diameter is d_s. The following dimensionless parameters completely define pad geometry and supply hole position:

$$\alpha = \frac{l}{L_x}$$
$$\beta = \frac{L_y}{L_x} \qquad (1)$$
$$\gamma = \frac{w}{l}$$

α is the dimensionless parameter that indicates the distance of the supply holes from the edges of the pad. β is the aspect ratio of the pad and γ is the ratio of the distance between the holes referred to the distance from the edges. L_x is assumed to be greater than L_y, so $0 < \beta < 1$. Coefficient α is defined in the range $0 < \alpha < \beta/2$. Case α=0 is not realistic, as the supply hole would be in correspondence of the pad edge. Case $\alpha = \beta/2$ is not realistic too as two rows of holes would coincide in only one row positioned at the center axis of the pad. Given these three parameters, the number of holes N_x and N_y along the *x* and *y* directions is defined by formulas (2):

$$N_x = \frac{1 - 2\alpha}{\gamma\alpha} + 1$$
$$N_y = \frac{\beta - 2\alpha}{\gamma\alpha} + 1 \qquad (2)$$

The total number of supply holes is $2N_x+2N_y-4$. The minimum number of supply holes in this model is 4.

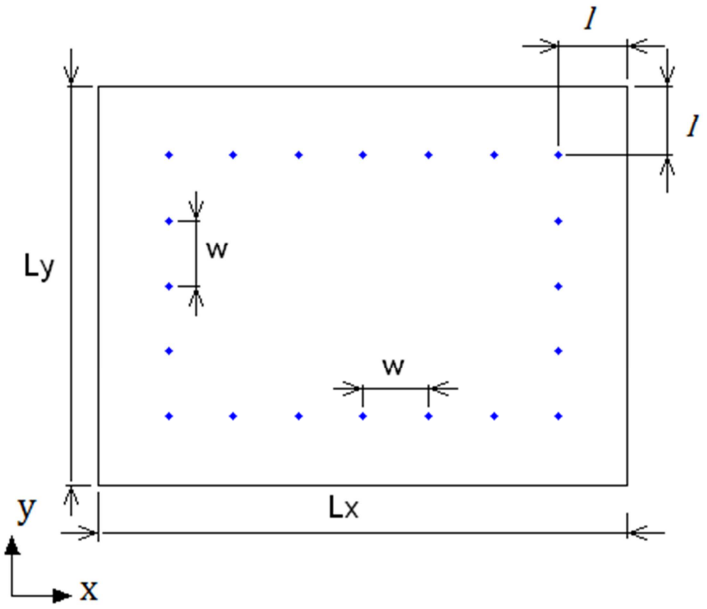

Figure 1: Sketch of the pad geometry under investigation

3. Distributed parameters model

The dimensionless form of the Reynolds equation for gas-lubricated bearings in steady conditions (3) is solved for the pads under investigation,

$$\frac{\partial}{\partial X}\left(PH^3\frac{\partial P}{\partial X}\right)+\frac{\partial}{\partial Y}\left(PH^3\frac{\partial P}{\partial Y}\right)=0 \tag{3}$$

where $X=x/L_x$, $Y=y/L_x$, $H=h/h_{ref}$, $P=p/p_a$. h_{ref} is the reference air gap, assumed equal to 10 μm.

A flow term at the input orifices is added to eq. (3). Pad input flow is the sum of the contributions of each supply hole. It can be easily approximated by an ellipse in the subsonic regime using ISO 6358 formula [40]

$$G = C\ k_T \rho_0 p_s \sqrt{1-\Phi^2} \tag{4}$$

where C is the conductance of each supply hole, ρ_0 is the air density in normal conditions (p_0=100 kPa and T_0=293.5 K), Φ is a coefficient that depends on the pressure ratio across the supply hole and $k_T=\sqrt{\frac{T_0}{T}}$ a temperature ratio. The expression of the conductance is

$$C=\pi\frac{d_s^2}{4}\frac{\Psi c_d}{\rho_0}$$

where, considering isentropic expansion, see [40], we have

$$\Psi=\frac{0.685}{\sqrt{R\cdot T}}$$

In case of subsonic flow ($b<\frac{p_c}{p_s}<1$), we have

$$\Phi=\frac{p_c/p_s-b}{1-b}$$

and for sonic flow ($p_c/p_s<b$) it is Φ=0, where p_c is the pressure downstream of the supply hole and b is the critical pressure ratio.

The discharge coefficient depends on the geometry of the supply orifice, as it is well known, see [41]. In our model the discharge coefficient c_d is assumed to be a function of ratio h/d_s and of the Reynolds number calculated at the supply hole cross section:

$$c_d=0.85\left(1-e^{-8.2\frac{h}{d_s}}\right)(1-0.3e^{-0.001Re}) \tag{5}$$

where Re is the Reynolds number calculated in the supply hole cross section:

$$Re=\frac{4G}{\pi\mu d_s}$$

This formula was experimentally obtained by testing different geometries (ratio h/d_s) and regimes (Re) of the supply holes [24]. It is the result of an extensive set of experimental tests carried out with supply holes of different diameters, by changing the air gap height and the supply pressure. The formula was adapted also to

microholes [36]. The DP model was substantiated by a comparison with experimental measurements carried out on rectangular pads with microholes [38] and on circular pads [39] and the accuracy is good.

Steady state lumped parameters model

A lumped parameters model was developed to simplify pad calculation and avoid solving the Reynolds equation with a numerical program developed for this purpose. This lumped model makes calculating pad characteristics faster and simpler.

The steady state model is based on the mass balance applied to the air volume inside the supply rectangle (see Figure 2):

$$G_{in} = G_{out} \tag{6}$$

where

$$G_{out} = 2(G_x + G_y) \tag{7}$$

The input flow is

$$G_{in} = c_1 c_d \, p_s \sqrt{1 - \Phi^2} \tag{8}$$

where

$$c_1 = \Psi \frac{\pi d_s^2}{4}\left(2N_x + 2N_y - 4\right)$$

Using the dimensionless parameters it is possible to obtain

$$c_1 = \Psi \frac{\pi d_s^2}{4}\left(\frac{2 + 2\beta - 8\alpha}{\alpha\gamma}\right) \tag{9}$$

The exhaust mass flow G_{out} can be calculated integrating along the edges of the supply rectangle the mass flow g per unit of length. This flow is expressed by the well-known formula for rectangular air channels, in case of isothermal viscous flow:

$$g = \frac{h^3}{24\mu RT}\frac{p_{in}^2 - p_{out}^2}{l}$$

where l is the length of the channel.
Using this formula we obtain the flow along x and y directions:

$$G_x = \frac{h^3}{24\mu RT}(p_0^2 - p_a^2)\frac{L_y - 2l}{l}$$
$$G_y = \frac{h^3}{24\mu RT}(p_0^2 - p_a^2)\frac{L_x - 2l}{l}$$

The total flow is

$$G_{out} = 2G_x + 2G_y$$
$$G_{out} = \frac{h^3}{12\mu RT}(p_0^2 - p_a^2)\left(\frac{L_y - 2l}{l} + \frac{L_x - 2l}{l}\right)$$

Introducing the dimensionless parameters α, β and γ we obtain

$$G_{out} = \frac{h^3}{12\mu RT}(p_0^2 - p_a^2)\left(\frac{\beta L_x}{l} + \frac{L_x}{l} - 4\right)$$

$$G_{out} = \frac{h^3}{12\mu RT}(p_0^2 - p_a^2)\left(\frac{\beta}{\alpha} + \frac{1}{\alpha} - 4\right)$$

The exhaust mass air flow G_{out} is finally:

$$G_{out} = c_2 h^3 (p_0^2 - p_a^2) \tag{10}$$

where

$$c_2 = \frac{1 + \beta - 4\alpha}{\alpha}\frac{1}{12\mu RT} \tag{11}$$

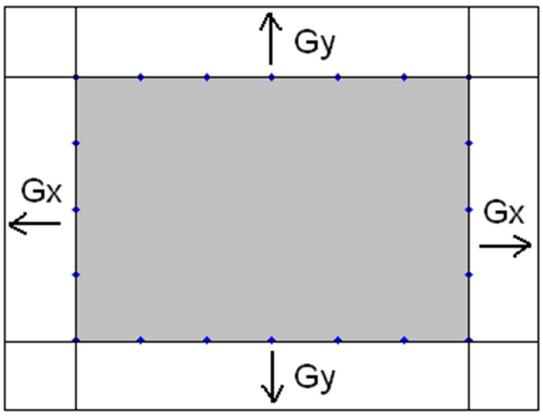

Figure 2: Region to which the mass balance is applied; in gray the supply rectangle is indicated

Pressure p_0 is the mean pressure calculated along the edges of the supply rectangle. The value calculated at the two sides is very similar for the geometry depicted in Figure 1, as distance *w* and length *l* are the same in both directions. Pressure p_0 is lower than the downstream pressure p_c. A similar definition for journal bearings was given in paper [37].

In this model, the supply hole downstream pressure p_c and the mean pressure p_0 are the two unknown quantities. To solve the problem, another formula relating the two pressures must be taken into account. For this purpose, ratio p_0/p_c was calculated with the DP model and a formula was identified (see the next paragraph) for use in the LP model.

The pad load carrying capacity *F* is estimated by considering constant pressure p_0 inside the supply rectangle and a linear decrease outside to ambient pressure p_a. The pressure is integrated considering the contributions of the supply rectangle of surface $(L_x - 2l)(L_y - 2l)$, the rectangles in the sides, of surface $(L_x - 2l)l$ and $(L_y - 2l)l$ and the squares in the corners, of surface l^2, see Figure 1.

The force *F* is then

$$F = (p_0 - p_a)\left[(L_x - 2l)(L_y - 2l) + l(L_x - 2l) + l(L_y - 2l) + \frac{4}{3}l^2\right]$$

$$F = (p_0 - p_a)\left[L_x L_y - l\left(L_x + L_y\right) + \frac{4}{3}l^2\right]$$

The pad's dimensionless load carrying capacity $\bar{F}$ is given by

$$\bar{F} = \frac{F}{p_a \beta L_x^2}$$

in which $\bar{F}$ is the ratio between the load capacity and a reference force obtained by the product of ambient pressure and the pad surface area.

Introducing the dimensionless parameters α, β and γ it is

$$\bar{F} = \frac{F}{p_a \beta L_x^2} = (P_0 - 1)\frac{1}{\beta L_x^2}\left[L_x^2\beta - lL_x(1+\beta) + \frac{4}{3}l^2\right]$$

$$\bar{F} = (P_0 - 1)\left[1 - \alpha\left(1 + \frac{1}{\beta}\right) + \frac{4\alpha^2}{3\beta}\right] \tag{12}$$

Pressure P_0 is considered in this formula, as it was verified that the mean pressure inside the supply rectangle is very similar to the mean pressure calculated on the edges of this rectangle.
A dimensionless air consumption is introduced by formula

$$\bar{G} = \frac{G}{2\left(N_x + N_y - 2\right)\pi\frac{d_s^2}{4}\,\Psi\;0.85\,p_s} \tag{13}$$

in which the air flow is referred to the maximum air flow in sonic conditions and with discharge coefficient c_d equal to 0.85.

The algorithm for implementing the LP model is shown in the flow-chart of Figure 3.

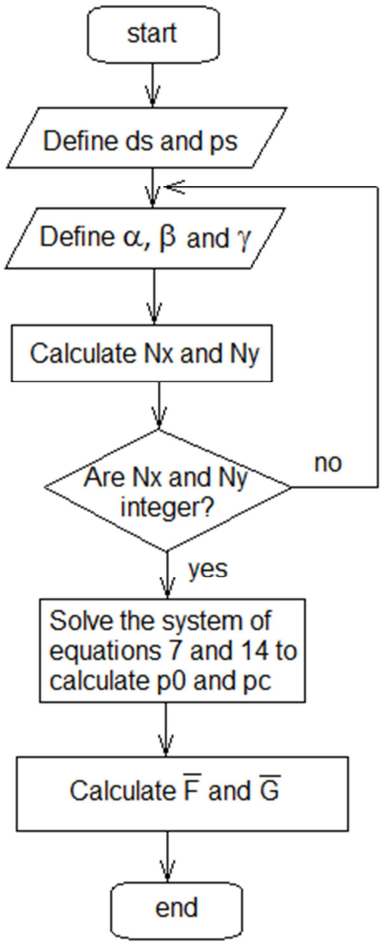

Figure 3: Flow-chart of the algorithm for implementing the LP model

4.1 Model identification

The distributed parameters (DP) model was used to calculate the mean pressure p_0 for different geometries, whose main geometric parameters are shown in Table 1. Pads A1 to C2 have an aspect ratio β=0.5, while pads D1 to D3 have different values of aspect ratio β.

Table 1: Geometric parameters of the investigated pads

pad	A1	A2	B1	B2	B3	C1	C2	D1	D2	D3
α	0.0833	0.0833	0.125	0.125	0.125	0.167	0.167	0.167	0.125	0.083
β	0.5	0.5	0.5	0.5	0.5	0.5	0.5	1	0.75	0.33
γ	2	1	2	1	0.667	1	0.5	1	1	1
N_x	6	11	4	7	10	5	9	5	7	11
N_y	3	5	2	3	4	2	3	5	5	3

Two expressions were found to approximate ratio p_0/p_c:

$$\frac{p_0}{p_c} = f_1\left(\gamma, \frac{1-2\alpha}{\beta-2\alpha}\right) = -0.134\gamma + 0.0044\frac{1-2\alpha}{\beta-2\alpha} + 0.97 \quad (14a)$$

or more simply

$$\frac{p_0}{p_c} = f_2(\gamma) = -0.148\gamma + 1 \quad (14b)$$

Parameter

$$\frac{L_x - 2l}{L_y - 2l} = \frac{1-2\alpha}{\beta-2\alpha}$$

is the aspect ratio of the supply rectangle. The coefficients of these expressions were calculated with the least square error minimization approach. Table 2 compares these formulas with the pressure ratio p_0/p_c obtained with the DP model.

The first expression takes the effect of the supply rectangle aspect ratio into account. For example, if we consider the geometries with γ=1, it can be seen that ratio p_0/p_c decreases when the supply rectangle ratio $\frac{1-2\alpha}{\beta-2\alpha}$ is increased. The second formula neglects this effect and is simpler. In any case, the error is less than 5% for any combination of parameters α, β and γ.

Table 2: Comparison between ratio p_0/p_c obtained with DPM and formulas f_1 (14a) and f_2 (14b)

pad	γ	$(1-2\alpha)/(\beta-2\alpha)$	DPM	f_1	error %	f_2	error %
A1	2	2.5	0.73	0.713	-2.3	0.704	-3.6
A2	1	2.5	0.87	0.847	-2.6	0.852	-2.1
B1	2	3	0.7	0.715	2.2	0.704	0.57
B2	1	3	0.85	0.849	-0.1	0.852	0.24
B3	0.667	3	0.9	0.894	-0.7	0.901	0.11
C1	1	4	0.81	0.854	5.4	0.852	5.2
C2	0.5	4	0.92	0.921	0.1	0.926	0.65
D1	1	1	0.82	0.840	2.5	0.852	3.9
D2	1	1.5	0.85	0.843	0.9	0.852	0.24
D3	1	5	0.875	0.858	-1.9	0.852	-2.6

4. Results and discussion

The pads were simulated with both LP and DP models considering the dimensionless air gap in the range 0.4<*H*<1.6 and a dimensionless supply hole diameter in the range 5<$\overline{d_s}$<30. This parameter is defined by

$$\overline{d_s} = \frac{d_s}{h_{ref}} \quad (15)$$

An example of 3D pressure distribution obtained with DP model is shown in figure 4. It is the case of pad C1 with *P*=6 and $\overline{d_s}$=10.

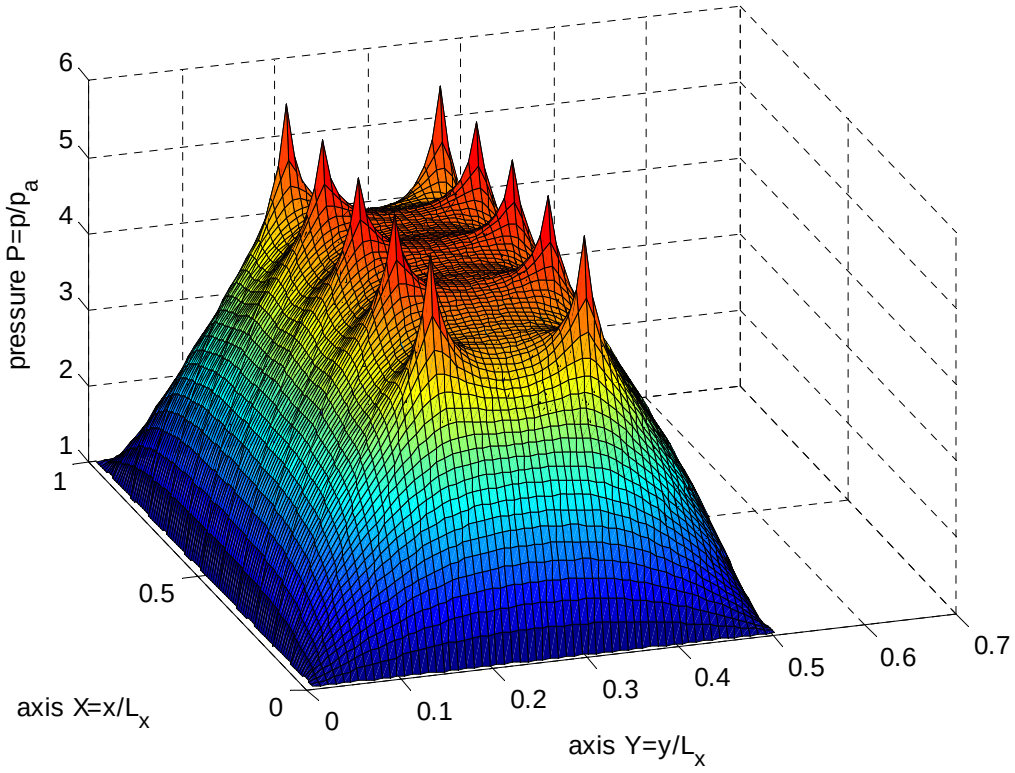

Figure 4: 3D pressure distribution for pad C1 with P=6 and $\overline{d_s}$=10 obtained with DP model

Figure 5 compares the dimensionless pressure distribution along the X direction at different air gaps, obtained with DP model. In calculations, h_{ref}=10 μm. As can be seen, the pressure distribution is almost independent of the air gap. The maximum relative difference of ratio p_0/p_c respect to the value obtained at H=1 is less than 6% for all pads considered (see Table 3). This explains why the air gap is not considered in eqs. 14.

Table 3: Ratio p_0/p_c at different air gaps and maximum relative difference respect to the values at H=1

	p_0/p_c			relative error	
pad	***H*=0.4**	***H*=1**	***H*=1.6**	***H*=0.4**	***H*=1.6**
A1	0.723	0.723	0.759	0.0%	5.0%
A2	0.869	0.865	0.872	0.5%	0.8%
B1	0.677	0.692	0.73	-2.2%	5.5%
B2	0.8473	0.843	0.854	0.5%	1.3%
B3	0.899	0.895	0.9	0.4%	0.6%
C1	0.822	0.804	0.81	2.2%	0.7%
C2	0.922	0.92	0.925	0.2%	0.5%
D1	0.824	0.817	0.827	0.9%	1.2%
D2	0.846	0.84	0.848	0.7%	1.0%
D3	0.87	0.8695	0.88	0.1%	1.2%

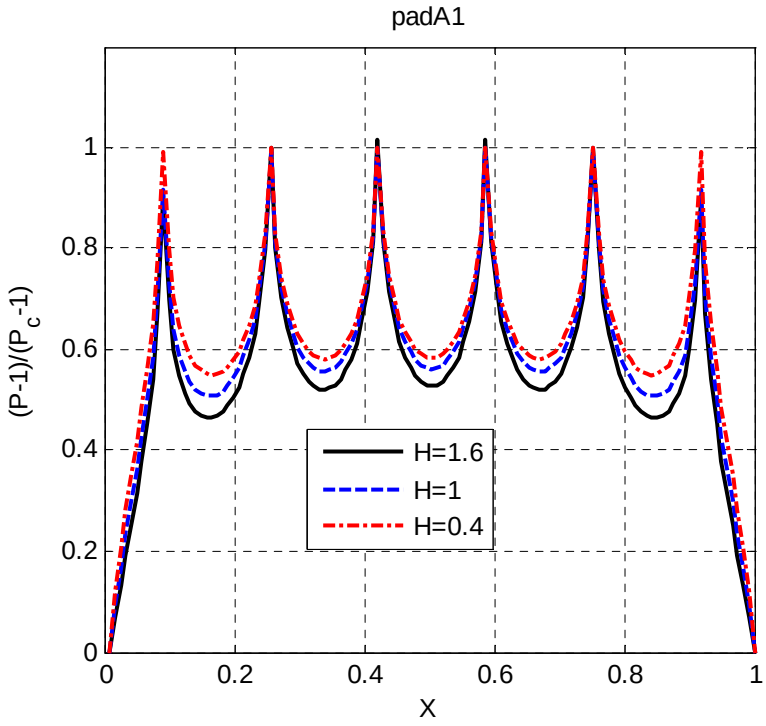

Figure 5: Dimensionless pressure distribution for pad A1 in case H=1.6, 1 and 0.4; $P_s=p_s/p_a$=6, $\bar{d}_s$=10.

If pads with different ratios γ are compared, it is clear from Table 2 that ratio p_0/p_c decreases when γ is increased, as in the case of pads B1, B2 and B3. This occurs when the distance w between the supply holes is increased or the distance l from the pad edges is decreased. In the range $0.5 < \gamma < 2$, this relationship is almost linear. In Figure 6, ratio p_0/p_c is compared for all pads with formula 14b. This formula provides a good approximation of the results obtained with the DP model in the range γ<3. It was found that this behavior is no longer linear outside this range.

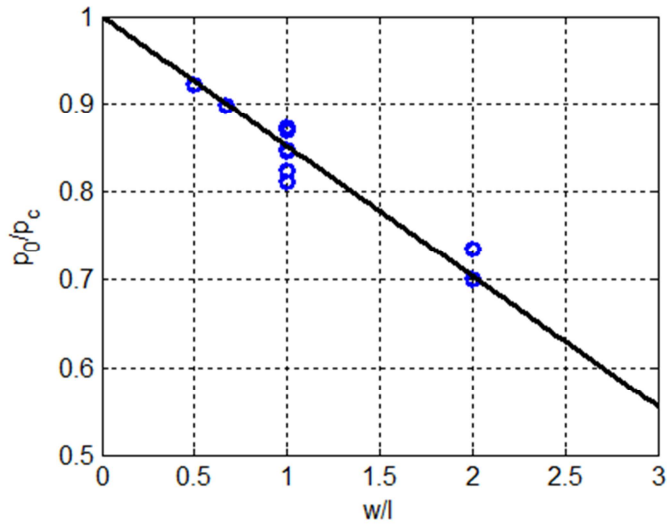

Figure 6: Ratio p_0/p_c vs γ=w/l for the pads under investigation

If pads with the same ratio γ=w/l are compared, e.g., pads A2, B2 and C1, p_0/p_c decreases when ratio $\frac{1-2\alpha}{\beta-2\alpha}$ is increased. These pads are shown in Figure 7a, while their pressure distribution is compared in Figure 7b.

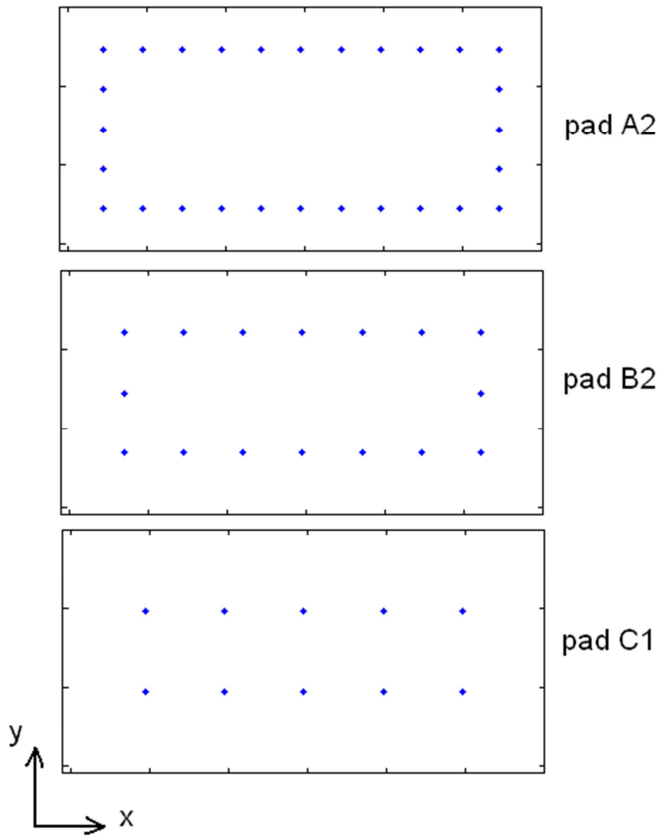

Figure 7a: Sketch of pads A2, B2 and C1; γ=1, $\bar{d}_s$=10.

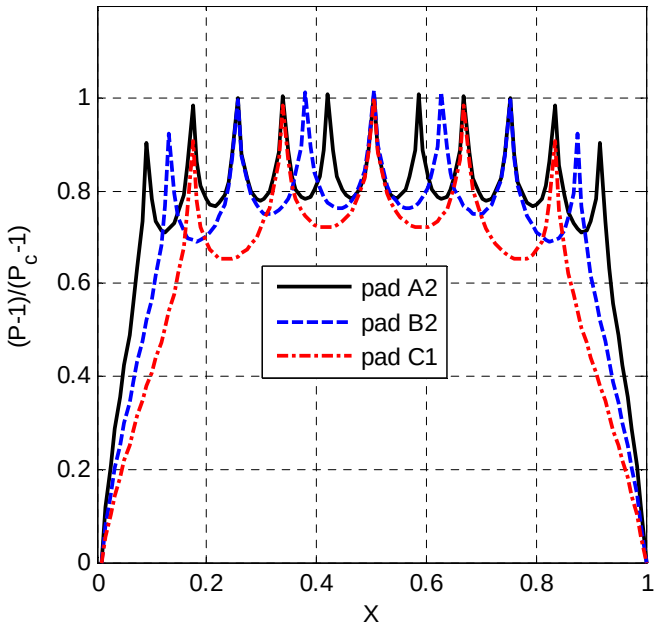

Figure 7b: Dimensionless pressure distribution for pads A2, B2 and C1; γ=1, P_s=6, $\bar{d}_s$=10.

The results for pads D1 to D3 show that ratio p_0/p_c increases as aspect ratio β decreases (if ratio γ is kept constant, see Table 2).

The results from the model are practically independent of supply pressure p_s. As Figure 8 shows, dimensionless pressure distribution was found to be almost identical at different supply pressures in the common range of operation (6<P_s<11).

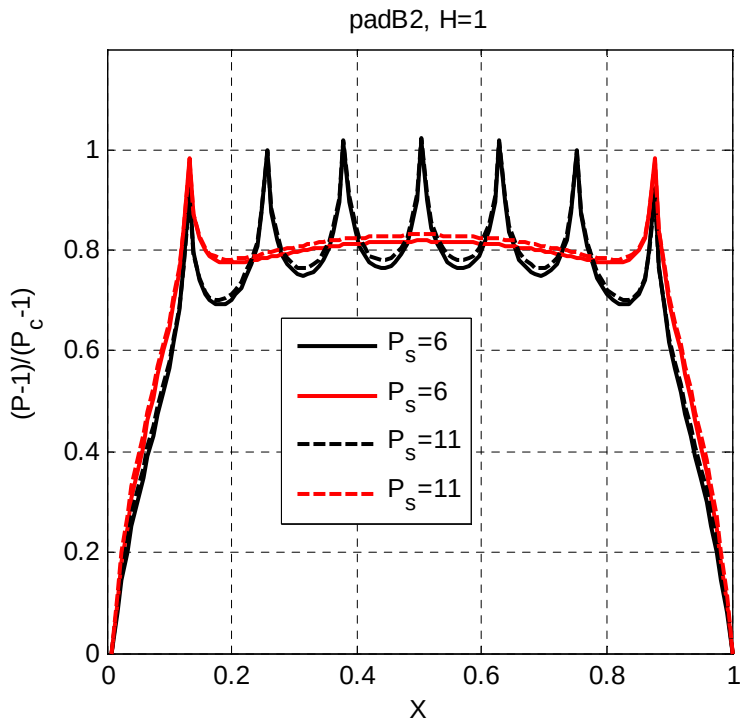

Figure 8: Dimensionless pressure distribution for pad B2, H=1, $\bar{d}_s$=10; comparison between P_s=6 and 11

Moreover, supply hole diameter has a negligible effect on ratio p_0/p_c in the range 5<$\bar{d}_s$<30. Dimensionless pressure distributions in two different planes are compared in Figure 9.

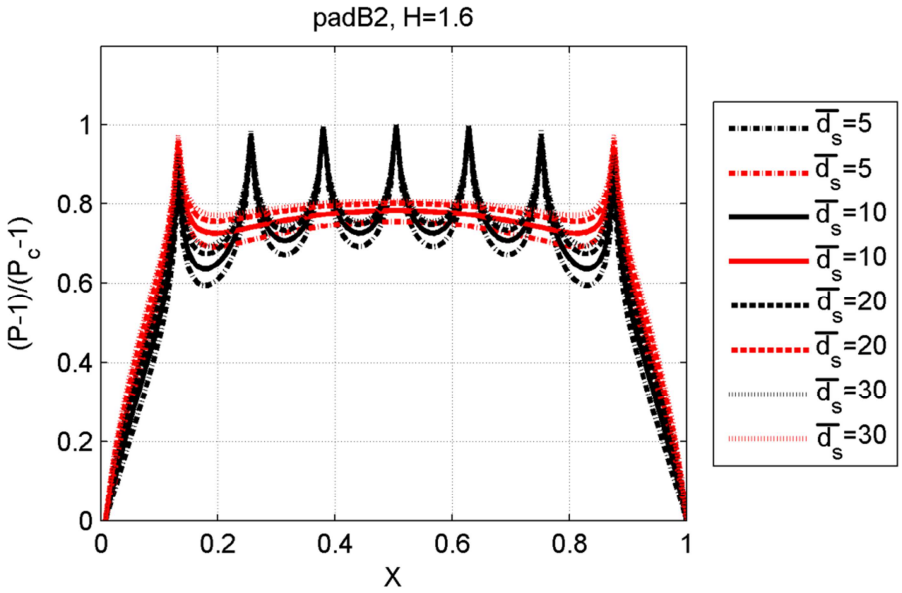

Figure 9: Dimensionless pressure distribution for pad B2, H=1.6, P_s=6; comparison between $\bar{d}_s$=5, 10, 20 and 30

The load carrying capacity and air consumption obtained with the DP and the LP models were compared for all pads. The LP model agrees quite well with the DP model. As an example, Figure 10 compares the dimensionless load capacity and air consumption for pads A1, B1 and C1, depicted in Figure 11. For load capacity in the H=0.4 to 1.6 range, the LP model gives a maximum relative error with respect to the DP model of less than 12%, while the error for air consumption is less than 10% (see Table 4). In most cases, the maximum errors for load capacity are for H=0.4.

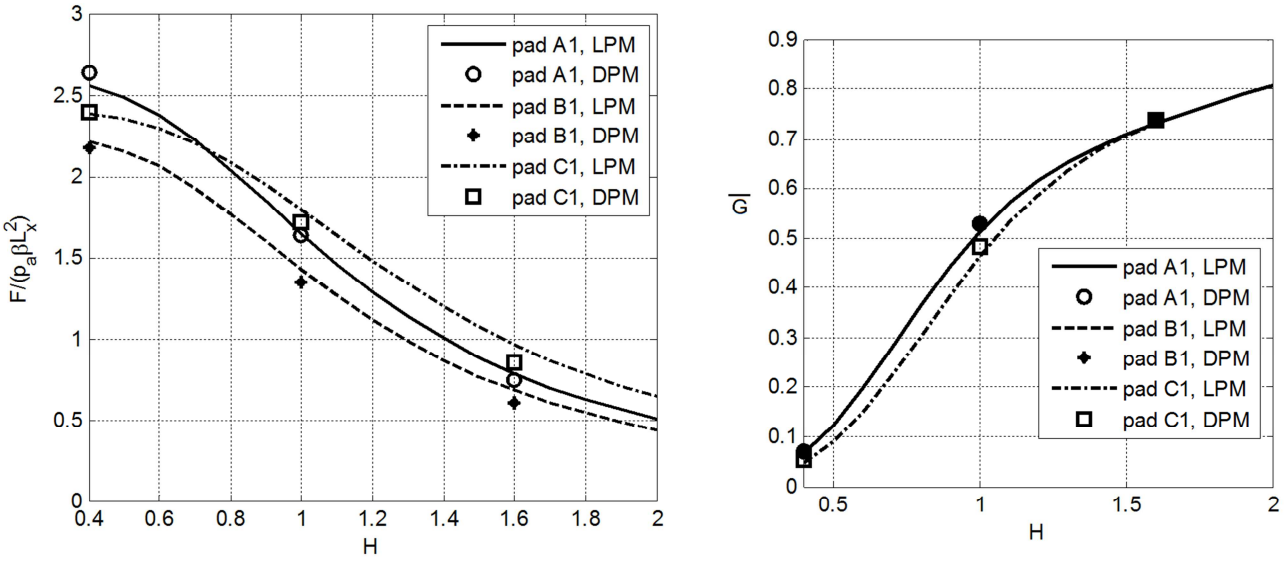

Figure 10: Dimensionless load capacity and air flow for pads A1, B1 and C1, P_s=6; comparison between LP and DP models

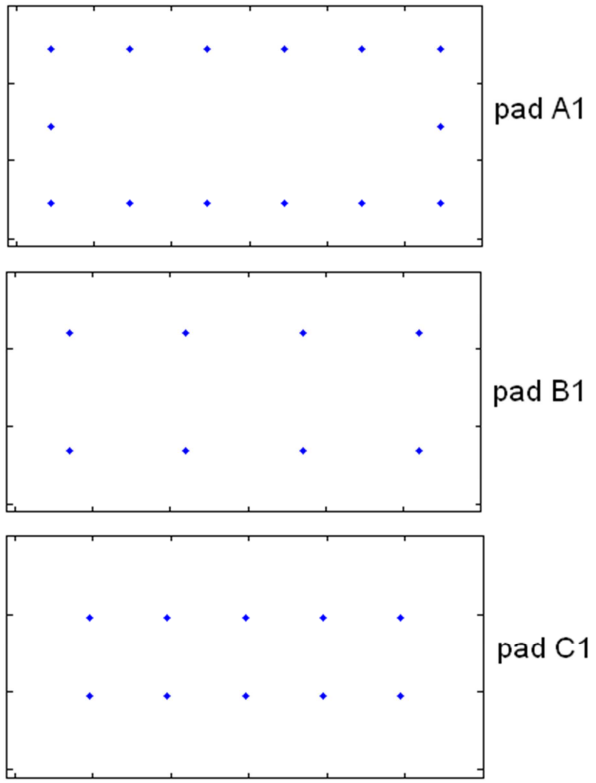

Figure 11: Sketch of pads A1, B1 and C1

Table 4: Relative error for the LP model with respect to the DP model in estimating load capacity and air consumption

pad	max. error for *F*	max. error for *G*
A1	-3.16%	-3.28%
A2	-4.80%	-3.62%
B1	1.79%	-2.76%
B2	-2.92%	-3.50%
B3	-5.50%	-5.76%
C1	12.34%	-4.18%
C2	-6.15%	-9.74%
D1	5.72%	-2.28%
D2	-2.02%	-2.78%
D3	-6.61%	-3.93%

The LP model approximates the DP model better than the models shown in ref. [35], of which this model is an evolution. The improvement stems from having introduced two different pressures (p_0 and p_c) related by formula 14, instead of considering the same pressure in calculating G_{in} and G_{out}.

5. Influence of parameters on pad performance

The LP model was then used to evaluate the influence of parameters α, β, γ and $\bar{d}_s$ on load capacity, stiffness and air consumption. The dimensionless variables were calculated; in particular, dimensionless stiffness is defined by

$$\bar{k} = k\frac{h_{ref}}{p_a \beta L_x^2} \tag{16}$$

One parameter at a time was changed within the following ranges of variation:

$0.5<\gamma<2$

$0.5<\beta<1$

$\beta/10<\alpha<2\beta/5$

with the restriction that the number of holes N_x and N_y be an integer.

Case 1: $\gamma=1$; $\beta=0.5$; $0.05<\alpha<0.2$

The possible values of α are shown in Table 4, which also indicates N_x and N_y. Figure 12 shows dimensionless load capacity, stiffness and air consumption of pads with different α values. Sketches of the first and the last pads in Table 4 are also given. When α is decreased, the supply holes increase in number and move towards the edges of the pad.

Table 4: Geometrical parameters in case 1

α	1/6	1/8	1/10	1/12	1/14	1/16	1/18	1/20

N_x	5	7	9	11	13	15	17	19
N_y	2	3	4	5	6	7	8	9

It is clear that pad load carrying capacity and stiffness increase when coefficient α is decreased. The air gap at which stiffness is maximum is around $h=h_{ref}$ and does not change with α. Dimensionless air consumption is independent of coefficient α. The flow rate is proportional to the total number of supply holes; this means that the air flow through each hole does not change when parameter α is modified. The supply hole downstream pressure p_c thus remains unchanged.

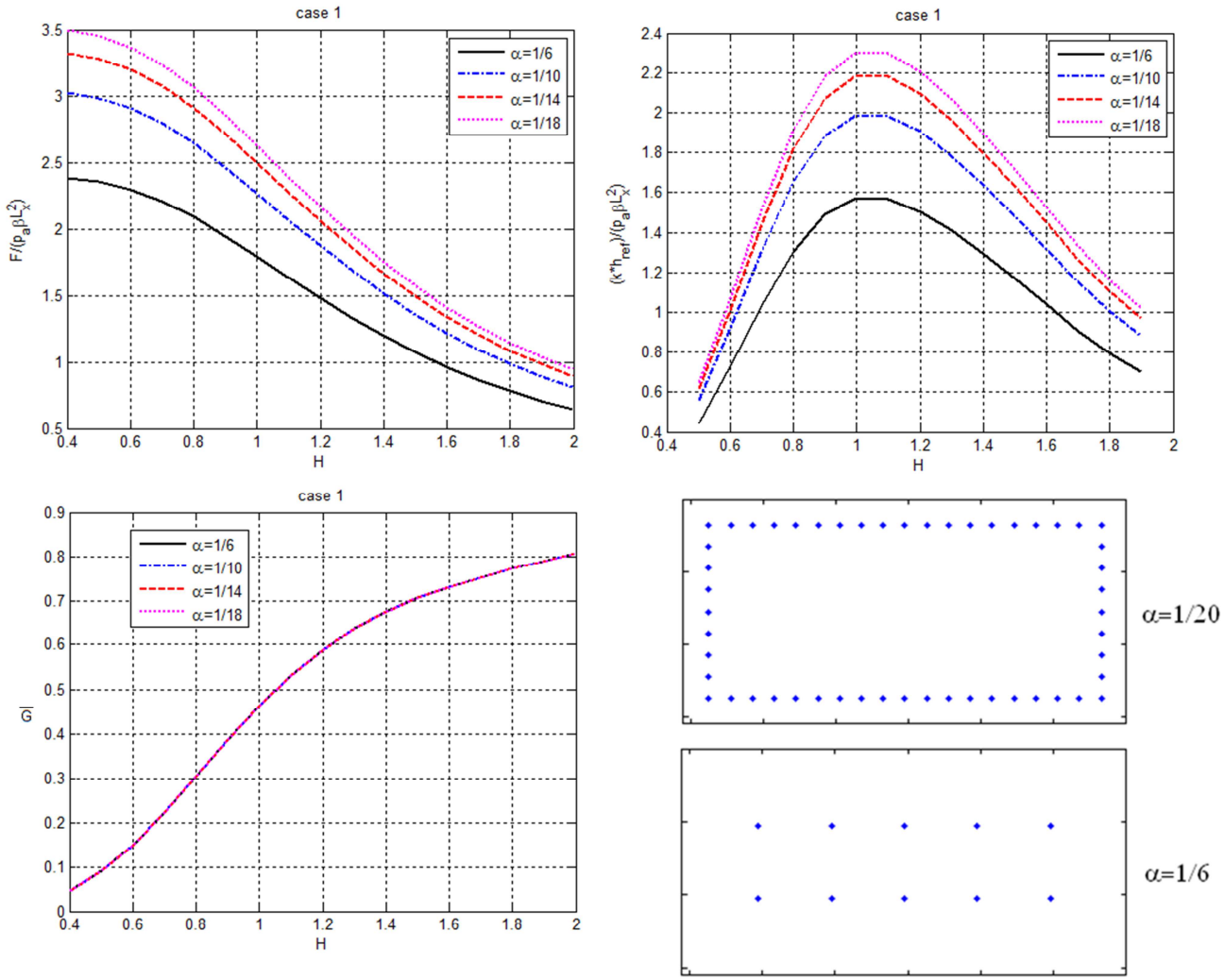

Figure 12: Dimensionless load capacity, stiffness and air consumption of pads with different α values; sketch of the first and last pads in Table 4

Case 2: α=0.125; γ=1; 0.5<β<1

The possible values of β are shown in Table 5, which also indicates N_x and N_y. Figure 13 shows the characteristics of pads with different β values, as well as a sketch of the first and the last pads in Table 5.

Table 5: Geometrical parameters in case 2

β	1/2	5/8	3/4	7/8	1
N_x	7	7	7	7	7
N_y	3	4	5	6	7

It is clear from Figure 13 that load capacity and stiffness increase when ratio β approaches unity. A square pad is to be preferred to a rectangular pad with the same surface area. As in the previous case, dimensionless flow rate is independent of ratio β.

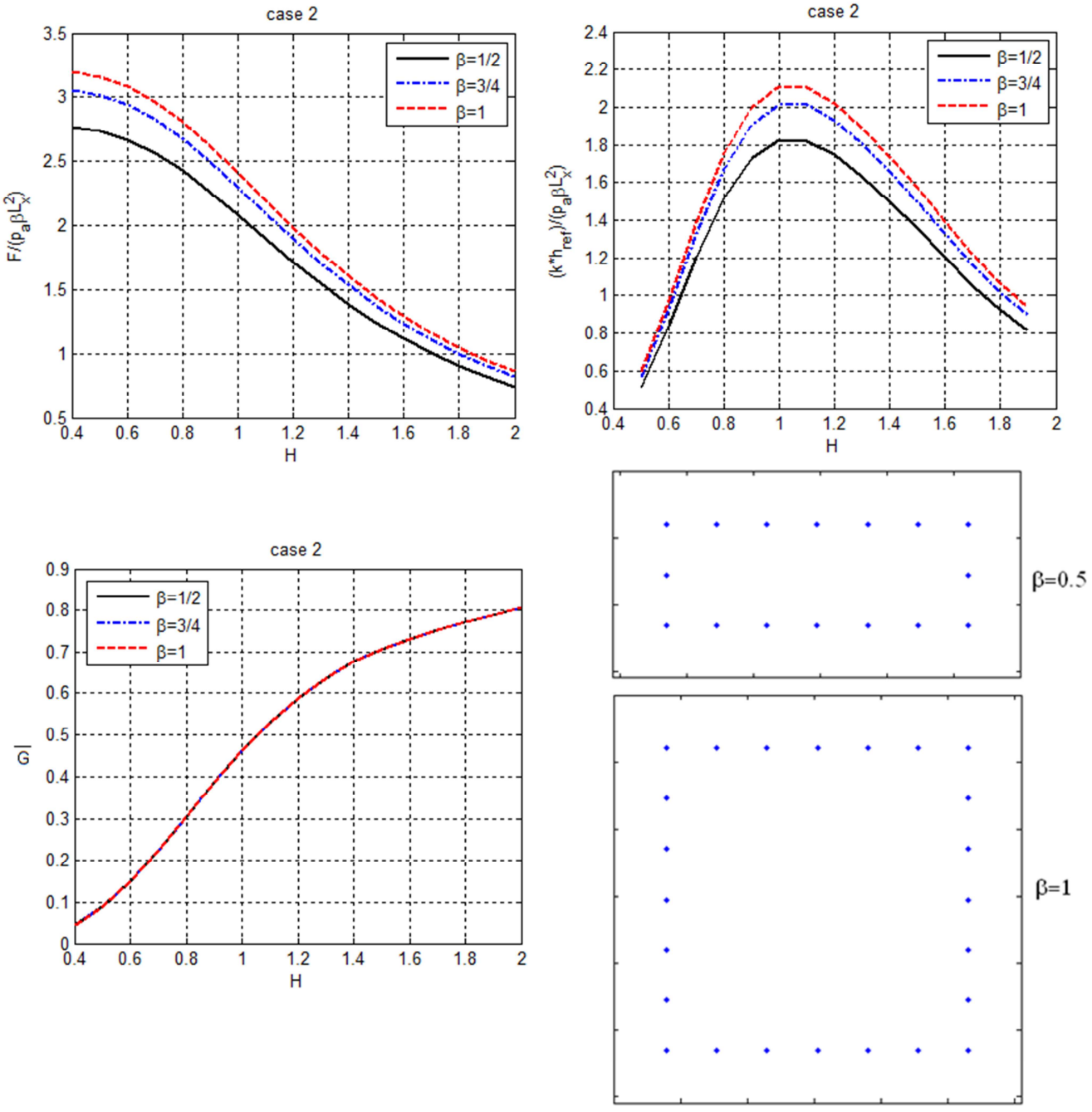

Figure 13: Dimensionless load capacity, stiffness and air consumption of pads with different β values; sketch of the first and last pads in Table 5

Case 3: α=0.125; β=0.5; 0.5<γ<2

The possible values of γ are shown in Table 6, which also indicates N_x and N_y. Figure 14 shows the characteristics of pads with different γ values, as well as a sketch of the first and the last pads in Table 6.

Table 6: Geometrical parameters in case 3

γ	1	2/3	1/2
N_x	7	10	13
N_y	3	4	5

Load capacity increases when ratio γ is decreased, but stiffness decreases. Air gap at maximum stiffness increases. As ratio p_0/p_c is a function of γ in this case, dimensionless flow rate is not independent of γ. Flow rate decreases along with γ.

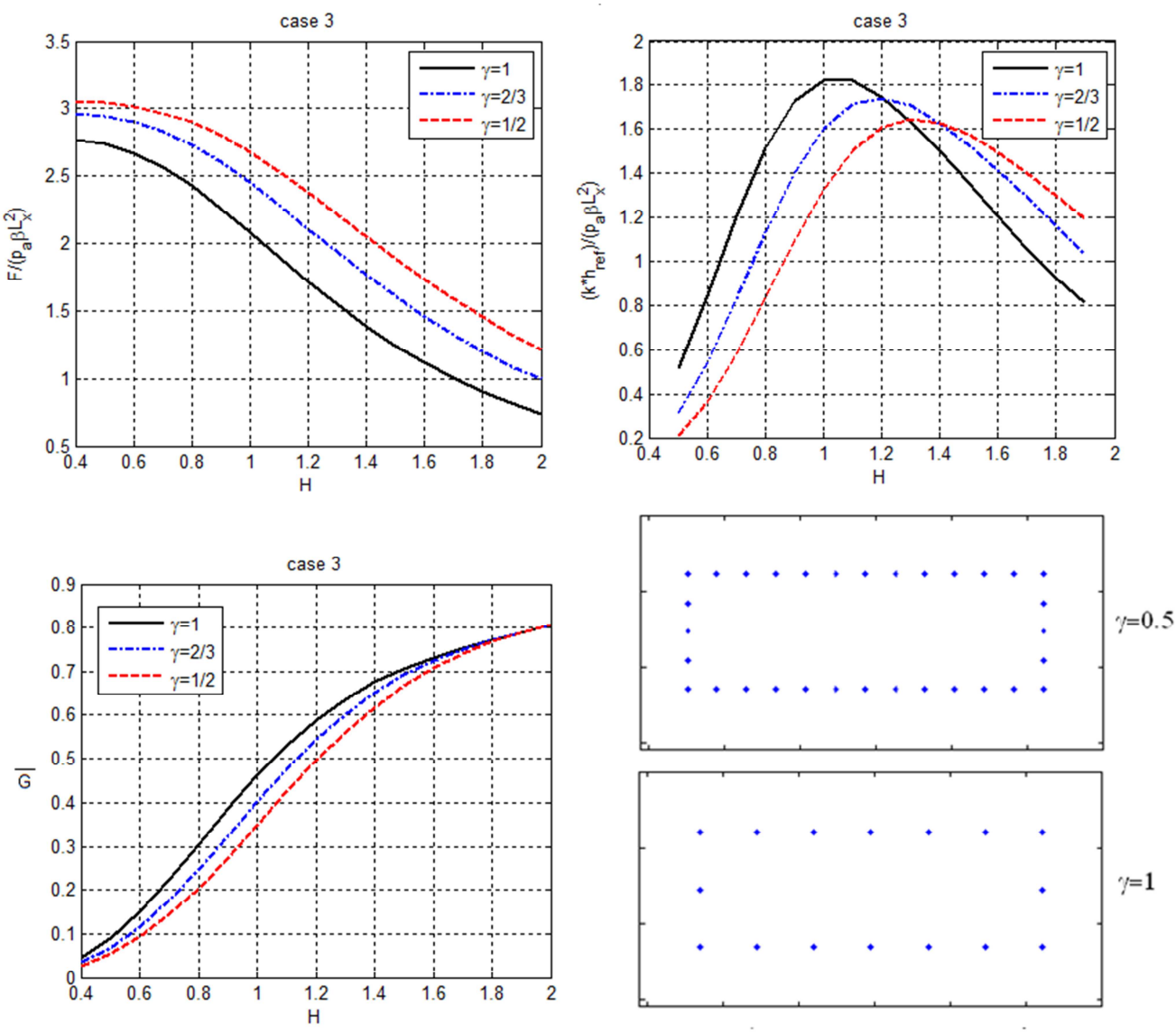

Figure 14: Dimensionless load capacity, stiffness and air consumption of pads with different γ values; sketch of the first and last pads in Table 6

Case 4: α=0.125; β=1; γ=1; 10<$\overline{d_s}$<20

In this case, N_x=7 and N_y=3. As diameter $\overline{d_s}$ is larger, load capacity increases, but stiffness decreases (see Figure 15). Air gap at maximum stiffness increases. Dimensionless air consumption decreases if the air gap is maintained constant; the same dimensionless air flow can be obtained at larger air gaps.

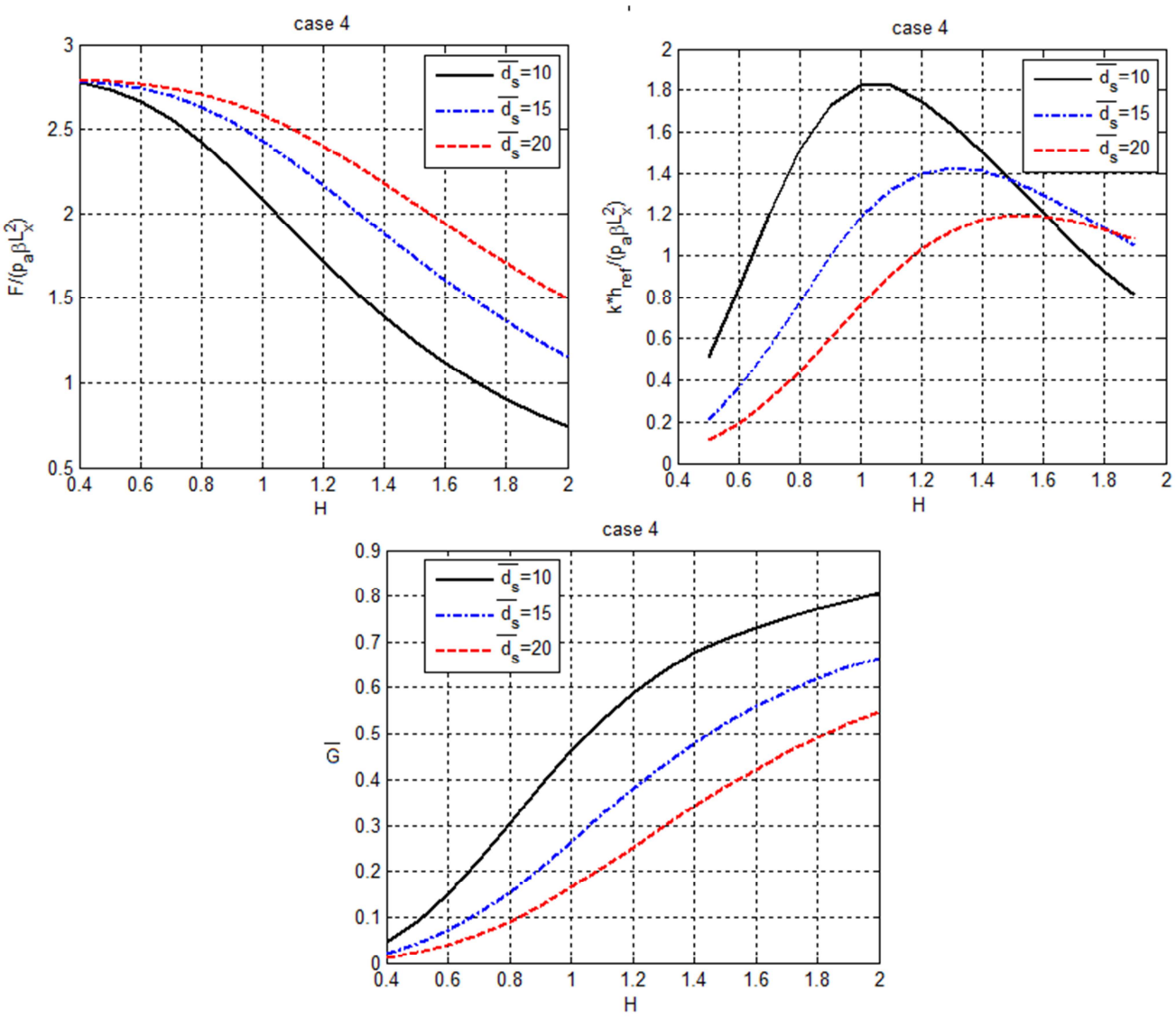

Figure 15: Dimensionless load capacity, stiffness and air consumption of pads with different d_s.

6. Conclusions

A lumped parameters model was developed to calculate the static performance of rectangular air pads. The model was compared with a distributed parameters model and was found to be sufficiently accurate and faster to implement. The model takes several dimensionless parameters into account which in combination define a general geometry. Analysis of a number of geometric parameters provided useful information for designing new pads. Main findings were as follows:

- It is advisable to increase the number of supply holes and move them towards the edges of the pad to increase load capacity and stiffness.

- The square pad maximizes load capacity and stiffness compared to a rectangular pad.
- Increasing ratio *w*/*l* decreases load capacity decreases, while stiffness also increases with air consumption.

As the LP model is a very good approximation with the DP model in many different geometries, we can affirm its general validity.

References

[1] J.S. Ausman. An improved analytical solution for self-acting, gas-lubricated journal bearings of finite length. Journal of Basic Engineering, vol. 83, June 1961, pp.188-194.

[2] D.C. Allais. The design of externally pressurized gas thrust bearings for maximum stiffness and stability. ASLE Transactions, vol. 5, 1962, pp.254-260.

[3] H. Mori, H. Yabe. Theoretical investigations of externally pressurized thrust collar gas-bearings. ASLE Transactions, vol. 6, April 1963, pp.337-345.

[4] H. Mori, H. Yabe, T. Ono. Theory of externally pressurized circular thrust porous gas bearing. Journal of Basic Engineering, vol. 87, September 1965, pp.613-621.

[5] Mori, H., Miyamatsu, Y. Theoretical flow-models for externally pressurized gas bearings. ASME Journal of lubrication technology, vol. 91, January 1969, pp. 181-193.

[6] M.P. Robert, F. Hendriks. Gas optimization of an externally pressurized air bearing. Tribology Transactions, vol. 33, 1, 1990, pp.41-47.

[7] J.S. Plante. J. Vogan, T. E. Aguizy, A.H. Slocum. A design model for circular porous air bearings using 1D generalized flow method. Precision Engineering, vol. 29, 2005, pp.336-346.

[8] K.J. Stout, S. El-Ashkar, V. Ghasi, M. Tawfik. Theoretical analysis of two configurations of aerostatic flat pad bearings using pocketed orifice restrictors. Tribology International, vol. 26, 1993, pp. 265-273.

[9] H. Zhang, C. Zhu, Q. Yang, Approximate numerical solution of hydrodynamic gas journal bearings, ICIRA 2008, Part II, LNAI 5315, pp. 260–268, 2008, Springer-Verlag Berlin Heidelberg.

[10] Y.S. Chen, C.C. Chiu, T.D. Cheng. Influences of operational conditions and geometric parameters on the stiffness of aerostatic journal bearings. Precision Engineering, vol.34, 2010, pp. 722-734.

[11] G. Belforte, F. Colombo, T. Raparelli, A. Trivella, V. Viktorov. Comparison between grooved and plane aerostatic thrust bearings: static performance, Meccanica, vol 46, 2010, pp. 547-555.

[12] F. Colombo, M. Conte. Multi-Objective Optimization of a Rectangular Air Bearing by Means of Genetic Algorithms. Journal of Mechanics Engineering and Automation, 2012, 2, pp. 355- 364.

[13] M.Fourka, Y.Tian, M. Bonis. Prediction of the stability of air thrust bearings by numerical, analytical and experimental methods. Wear, vol. 198, 1996, pp.1-6.

[14] Y.T. Li, H. Ding. Design analysis and experimental study of aerostatic linear guideways used in a high acceleration and high precision xy stage. Proc. IMechE, vol. 221 Part J, Engineering Tribology, 2007.

[15] N. Bhat, S.M Barrans. Design and test of a Pareto optimal flat pad aerostatic bearing. Tribology International, vol. 41, 2008, pp.181-188.

[16] M.T. Neves, V.A. Schwarz, G.J. Menon. Discharge coefficient influence on the performance of aerostatic journal bearings. Tribology International, vol.43, 2010, pp.746-751.

[17] A. Charki, K. Diop, S. Champmartin, A. Ambari. Numerical simulation and experimental study of thrust air bearings with multiple orifices. International Journal of Mechanical Sciences, vol.72, 2013, pp.28-38.

[18] G. Aguirre, F.Al-Bender, H. V. Brussel. A multiphysics model for optimizing the design of active aerostatic thrust bearings. Precision Engineering, vol. 34, 2010, pp. 507-515.

[19] X.D. Chen, X.M. He. The effect of the recess shape on performance analysis of the gas-lubricated bearing in optical lithography. Tribology International, vol. 39, 2006, pp.1336-1341.

[20] S. Yoshimoto, M. Yamamoto, K. Toda. Numerical calculations of the pressure distribution in the bearing clearance of circular aerostatic thrust bearings with a single air supply inlet. Transactions of the ASME, vol.129, 4, 2007, pp.384-390.

[21] Y. Li, H. Ding. Influences of the geometrical parameters of aerostatic thrust bearing with pocketed orifice-type restrictor on its performance. Tribology International, vol. 40, 2007, pp.1120-1126.

[22] M.E. Eleshaky. CFD investigation of pressure depression in aerostatic circular thrust bearings. Tribology International, vol. 42, 2009, pp.1108-1117.

[23] M. Masaaki, S. Yoshimoto. Numerical investigation of static and dynamic characteristics of aerostatic thrust bearings with small feed holes. Tribology International, vol. 43, 2010, pp.1353-1359.

[24] G. Belforte, T. Raparelli, V. Viktorov. A. Trivella. Discharge coefficients of orifice-type restrictor for aerostatic bearings. Tribology International, 40, 2007, pp. 512-521.

[25] T. Waumans, F. Al-Bender, D. Reynaerts. A semi-analytical method for the solution of entrance flow effects in inherently restricted aerostatic bearings. Proceedings of GT2008 ASME Turbo Expo 2008: Power for Land, Sea and Air, June 9-13, 2008, Berlin, Germany.

[26] A. Andrisano, A. Maggiore. Theoretical and experimental analysis of an externally pressurized porous gas thrust bearing. Tribology International, vol. 10, 1978, pp. 285-288.

[27] Y. Li, H. Ding. A simplified calculation method on the performance analysis of aerostatic thrust bearing with multiple pocketed orifice-type restrictors, Tribology International, vol. 56, 2012, pp. 66-71.

[28] R. Bassani, E. Ciulli, P. Forte. Static behaviour of an integral externally pressurized gas bearing - comparison with other types of bearing. Tribology International, vol. 22, 3, 1989, pp. 177-188.

[29] S. Kassab. Performance of an externally pressurized rectangular gas bearing under constant effective recess pressure. Tribology International, 1994, vol. 27, pp. 159-167.

[30] T. Raparelli, V. Viktorov, A. Trivella. Static and dynamic analysis of pneumatic support. 7th International Workshop on Robotics in Alpe-Adria Danube region-RAAD 98, Slovakia, June 26-28, 1998, pp.405-410.

[31] E. Salem, M. Shawky. An experimental investigation into the performance of externally pressurized rectangular air bearings. Wear, vol.50, 1978, pp.237-257.

[32] K.V. Raman, B. Majumdar. Experimental investigation of the stiffness and damping characteristics of aerostatic rectangular thrust bearings. Wear, vol. 52, 1979, pp.71-78.

[33] H. Mori, H. Yabe, K. Ohnishi. Analysis of externally pressurized rectangular pads with multiple supply holes. ASLE Transactions, vol.9, 1966, pp. 391-401.

[34] G. Belforte, F. Colombo, T. Raparelli, A. Trivella, V. Viktorov. Lumped parameters models of pneumatic rectangular pads. Proceedings of XX Congresso Associazione Italiana di Meccanica Teorica e Applicata, Aimeta2011, Bologna 12-15 settembre, pp. 1371-1378.

[35] G. Belforte, F. Colombo, T. Raparelli, A. Trivella, V. Viktorov. Study of the static and dynamic performance of rectangular air pads by means of lumped parameters models. Proceedings of the 11th Biennial Conference on Engineering Systems Design and Analysis ESDA 2012, July 2-4, Nantes, France.

[36] ISO 6358-1, 2013. Pneumatic Fluid Power - Determination of flow-rate characteristics of components using compressible fluids - Part 1: General rules and test methods for steady-state flow.

[37] G. Belforte, F. Colombo, T. Raparelli, A. Trivella. V. Viktorov. Identification of micro-hole discharge coefficients for air bearings. 3rd European Conference on Tribology, Ecotrib 2011, June 7-9, 2011, Vienna, Austria, vol. 2, pp. 561-566.

[38] G. Belforte, F. Colombo, T. Raparelli, A. Trivella, V. Viktorov. Experimental Analysis of Air Pads with Micro-Holes. Tribology Transactions, 2013, Vol. 56, pp. 169-177.

[39] G. Belforte, T. Raparelli, A. Trivella, V. Viktorov. Identification of discharge coefficients of orifice-type restrictors for aerostatic bearings and application examples. New Tribological Ways, InTech, 2011, pp. 359-380.

[40] G. Belforte, T. Raparelli, V. Viktorov. Modeling and identification of gas journal bearings: self-acting gas bearing results. Journal of Tribology, vol. 124, 2002, pp. 716-724.

[41] J.W. Powell, Design of Aerostatic Bearings, The Machinery Publishing Co Ltd, 1970.